Department of Physics and Astronomy
University of Heidelberg

Bachelor Thesis in Physics
submitted by

Sophia Milanov

born in Düsseldorf (Germany)

2016

Hunting for intermediate-mass black holes: a new action-based approach

This Bachelor Thesis has been carried out by Sophia Milanov at the
Max Planck Institute for Astronomy in Heidelberg
under the supervision of
Dr. Glenn van de Ven

Abstract

Hello, here is some text without a meaning. This text should show what a printed text will look like at this place. If you read this text, you will get no information. Really? Is there no information? Is there a difference between this text and some nonsense like “Huardest gefburn”? Kjift – not at all! A blind text like this gives you information about the selected font, how the letters are written and an impression of the look. This text should contain all letters of the alphabet and it should be written in of the original language. There is no need for special content, but the length of words should match the language.

Contents

1 Introduction

Globular clusters (GCs) are self-gravitating, gas-free systems of 10^5 to 10^7 stars which are spherically grouped. There are about 150 of them in the Milky Way (MW) (Harris, 1996). Since they are some of the oldest stellar populations in the universe (approximately 13 Gyr), they contain much information about the assembly history and evolution of the MW. Formerly seen as very simple spherical and isotropic stellar systems with only one stellar population (Meylan and Heggie, 1997), recent research revealed a much higher degree of complexity (that differ in the light-elements abundances (Piotto *et al.*, 2015)). GCs are now known to host multiple stellar populations that challenge our understanding of their formation. Moreover, GCs now also appear dynamically complex, presenting deviations from spherical symmetry, anisotropy in velocity space and significant internal rotation (Zocchi *et al.*, 2012; Bianchini *et al.*, 2013; Kacharov *et al.*, 2014).

Recent attention has been devoted to the search of IMBHs in the centre of GCs. These elusive black holes $10^3\,M_\odot < M_\bullet < 10^4\,M_\odot$ could be the missing link between stellar mass black holes ($M_\bullet < 100\,M_\odot$) and super massive black holes (SMBHs, $M_\bullet > 10^5\,M_\odot$) as they could represent the seed for the formation of SMBHs. Their search in the centre of GCs has partially been motivated by the extrapolation of the $M_\bullet - \sigma$-relation for galaxies (Ferrarese and Merritt, 2000), describing the relation between the mass of a central massive black hole and the velocity dispersion of its host galaxy.

The hunt of IMBHs in Galactic GCs has been primarily based on two methods: 1) detection of radio and X-ray emission due to the accretion of gas in the black hole (Miller and Hamilton, 2002; Maccarone and Servillat, 2008; Kirsten and Vlemmings, 2012; Strader *et al.*, 2012); 2) detection of kinematic signatures in the central region of a GC (Bahcall and Wolf, 1976; Lützgendorf *et al.*, 2013). The first method proved to be difficult because the feeding of a black hole with gas is highly inefficient in a gas poor environment of Galactic GCs.

The kinematic detection of IMBHs is usually based on the analysis of the velocity-dispersion profile in the inner few arcseconds around the crowded centre of a GC in search for a rise of the dispersion. This requires a combination of high angular resolution and high spectral resolving power. For this reason the detection of IMBHs remains still highly controversial.

Currently there are two different kinematic methods trying to detect IMBHs: resolved kinematics & unresolved integrated light (see, for example Bianchini *et al.* 2015). These methods often deliver significant different results when applied to the same GC. As an

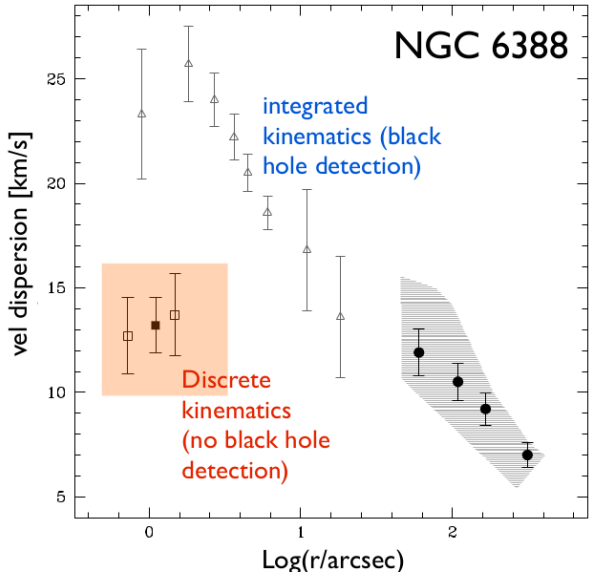

Figure 1: Velocity profile of NGC 6388 derived by the two different methods. We see a cusp given by the integrated kinematics method while there is no cusp with discrete kinematics. (Lanzoni *et al.*, 2013) and bianchini?

example there are the unresolved/integrated IFU kinematics which result in a signature of an IMBH for NGC 6388 (cusp in the velocity dispersion profile) (Lützgendorf *et al.*, 2011) and resolved/discrete kinematics which do not yield IMBHs (no cusp in the velocity dispersion profile)Lanzoni *et al.* (2013). Another example is ω centauri (van der Marel 2010, Noyola 2008).

Given these controversial results that prevent us from drawing definite conclusions on the existence of IMBHs in Galactic GCs we propose to introduce a new approach to analyse the effects of an IMBH to the central kinematic of a GC. Our method consists in going beyond the traditional phase space analysis (i.e., analysis of velocity dispersion profiles), by exploiting the orbital information of the stars. Our expectation is that an IMBH could alter the orbital properties of the stars that more closely interact with it.

An orbit is a path a unperturbed, collisionless tracer particle (e.g. a star) will move along in a gravitational potential. Orbits contain information about the gravitational potential generated by the mass distribution of a system in their position and velocity coordinates following Newtons 2nd law. Orbit distribution functions (DFs) describe which orbits are populated by how many tracers. From the orbit distribution function together with the overall potential we can draw inferences about the structure and evolution history of the system.

Historically observations of orbits enabled discoveries or confirmed them:

- Seen from the earth Mars' position moves over the sky as a loop called epicycle. That implies that the earth is not the centre of the universe! (Carroll and Ostlie, 2006, p.3)
- Neptune/Uranus noch mal nachlesen
- From rotation curves of galaxies we see that stars move faster than what expected by the presence of only the mass of luminous matter. There has to be more matter interacting via gravitational forces. This has led to the theory of dark matter. (Rubin 1980)
- Mercury's orbit differs hugely from calculated Kepler orbit. This is because of its migrating pericentre. Due to the proximity to the sun gravitational forces are so strong that we need to apply general relativity.
- The SMBH Sagittarius A* was detected by observations of the orbits around the black hole and resulting mass calculations. (Carroll and Ostlie, 2006, p.923)

Some examples for orbit DFs are spiral galaxies where stars of different components (thin disc, thick disc, bulge, halo) are on different orbits (dynamical distinct) and have different metallicities (chemical distinct).

Describing orbits with the coordinates $(\vec{x}(t), \vec{v}(t))$ is very difficult since they have a complicated time evolution in 6 coordinates. A better way to describe orbits are integrals of motion. They are constant along the orbit. The classical integrals of motion of a spherical system are energy and angular momentum. But in general the best choice of values to describe an orbit are actions which are as well integrals of motion. One of their advantages is that we can connect them with angle coordinates. They form together a set of canonical conjugate coordinates. Another advantage is that they have an intuitive explanation in contrary to the energy: they quantify the oscillation of the orbit in the different directions of the coordinates. That is why actions are excellent orbit labels and therefore ideal parameters for orbit DFs. Our goal is a description of DFs of GCs and due to above mentioned reasons we investigate in action space.

In this thesis we wish to test the feasibility of the analysis of the action/orbit space in GCs and test whether it could be possible to predict signatures of IMBHs. This

will be done by "translating" the traditional phase-space into orbit space, exploiting the potential and the $\vec{x}$ and $\vec{v}$ vectors. Although this type of information (6-D info) is not currently available for Galactic GCs we are motivated by the growing amount of photometric and kinematic data that are already able to deliver a 5-D info (2D spatial info and 3D kinematic info), in particular the high accuracy Hubble Space Telescope (HST) proper motions and the upcoming GAIA data. We will limit our analysis to GC simulations with and without IMBHs to explore our new approach. The thesis is structural in to parts: first we familiarize with a phase space analysis of the simulations and we will focus in how to study the orbits and extract predictions of the presence of an IMBH.

2 Method & Theory

2.1 Stellar population in GC

The typical stellar components of a GC can be seen in a color magnitude diagram (CMD). Figure 2 shows the CMD of a simulated GC where the visual magnitude is plotted against the B-V color. It's color coded by the mass of the star. A star's position can be

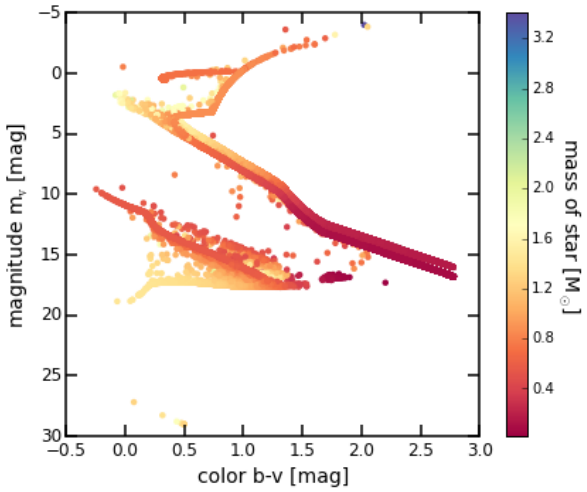

Figure 2: Color magnitude diagram of SIM 1.

interpreted as its evolution stage. Most of the stars are set in the main sequence. They fusion hydrogen in their cores. There are two main sequence lines one upon the other. These occur due to binary systems whose flux is given by the sum of the single fluxes of the single components, and therefore appear redder and more luminous. These binary systems represent about 5 % of the stars in the GC. The position of the main sequence turn-off depends on the age of the system and therefore can be used as an indicator to determine the cluster's age. Isochrones are curves of evolutionary stages of stars of a single stellar population (SSP) having the same age and metallicity but different masses. Bluewards of this turn off point following the trend of main sequence stars, there are so called "blue stragglers" which are remnants of stellar collisions or interacting binaries (Binney and Tremaine, 2008, p.628). Continuing from the turn off point there is the red giant branch consisting of stars still fusing hydrogen but only in a shell surrounding a degenerate helium core. They are inflated with a radius much higher than the main sequence stars but have a much lower surface temperature. These are the brightest stars of a GC. On the upper part of the red giant branch lies the horizontal branch. Its stars burn helium in their core and hydrogen in a surrounding shell. In the lower left

corner white dwarfs are located. They are stellar remnants which have burnt all of their resources. In a typical GC dark stellar remnants like stellar black holes and neutron stars are present but not visualised in the CMD.

2.2 Kinematic profiles of globular clusters

We will investigate GCs in phase space by analysing the stellar kinematic profiles (such as velocity dispersion and anisotropy profiles) and the spatial distribution of stars (density profiles and potential).

The stellar velocity dispersion quantifies the spread of different velocities stars at given positions can have. It is defined as the standard deviation of the velocity distribution

$$\sigma_{\mathrm{i}}(\mathrm{r}) \equiv \sqrt{\langle(\mathrm{v_i(r)} - \langle \mathrm{v_i(r)}\rangle)^2\rangle} = \sqrt{\langle \mathrm{v_i(r)}^2\rangle - \langle \mathrm{v_i(r)}\rangle^2} \qquad \mathrm{i} = \mathrm{r}, \theta, \phi. \tag{1}$$

Here v describes the actual velocity of the star while $\langle \mathrm{v} \rangle$ specifies the mean of the velocities of all considered stars. For a spherical system it is best to calculate them in spherical coordinates r, θ, ϕ respectively $\mathrm{v_r}, \mathrm{v}_\theta, \mathrm{v}_\phi$. If the GC contains an IMBH the velocity dispersion towards the centre is expected to increase.

To quantify the anisotropy of the system we use the anisotropy parameter β

$$\beta(\mathrm{r}) \equiv 1 - \frac{\sigma_\theta^2(\mathrm{r}) + \sigma_\phi^2(\mathrm{r})}{2\sigma_{\mathrm{r}}^2(\mathrm{r})} \tag{2}$$

taken from (Binney and Tremaine, 2008, eq. 4.61). If β is positive the anisotropy is radial, if it is negative the anisotropy is tangential and if $\beta \approx 0$ then the system is isotropic.

2.3 Density & potential

2.3.1 Density of a collisionless stellar system

We calculate the density by binning the masses on logarithmic equally distributed shells

$$\rho(\mathrm{r}) = \frac{\sum_{\mathrm{r=r_{in}}}^{\mathrm{r_{out}}} \mathrm{M(r)}}{\mathrm{V(r_{out} - r_{in})}} \tag{3}$$

with the sum of masses of stars with mass M(r) over a volume V which is taken from the radius of the inner shell $\mathrm{r_{in}}$ and the radius of the outer shell $\mathrm{r_{out}}$. We can considerGCs as quasi-collisional stellar system. The approximation of collisionless is motivated by

the fact that the dynamical time of a cluster is always shorter than the relaxation time $T_{dyn} < T_{relax} < T_{age GC} \equiv T_{Hubble}$. T_{dyn} is the time of a star to go from one side of the cluster to the other. This takes approximately 10^5 yr. The relaxation time is the time needed to redistribute energies of the stellar encounters and takes about 10^7 - 10^9 yr. The age of the GCs is approximately the Hubble time which is the age of the universe (10^10 yr). The first term motivates the collisionless approximation while the part starting with T_{relax} is telling us that a GC has lived for several relaxation times, therefore two-body interaction had time to act. That means in the long term that the system is collisional.

2.3.2 Generating the potential from Poisson's equation

Since the system is spherically potential and force only depend on the distance from the centre r. The potential Φ can be derived from the Poisson's equation

$$\Delta\Phi(r) = 4\pi G\rho(r) \tag{4}$$

with the gravitational constant $G = 6.674 \cdot 10^{-11}\,{}^{m^3}/_{kg\,s^2}$ (Mohr *et al.*, 2015) and the density ρ depending only on the distance as well. Due to the spherical symmetry the potential can be calculated by

$$\Phi(r) = -\frac{G}{r}\int_0^r dM(r') - G\int_r^\infty \frac{dM(r')}{r'} = -4\pi G\left[\frac{1}{r}\int_0^r dr' r'^2\rho(r') + \int_r^\infty dr' r'\rho(r')\right] \tag{5}$$

with dM describing the mass of spherical shells as proved by Binney and Tremaine (2008, eq. 2.28).

2.3.3 Other potential models

Kepler potential IMBH
Plummer model
short: isochrones

2.4 Orbits & integrals of motion

2.4.1 Classical integrals of motion in spherical potential

how does the orbit in a spherical potential look In a dynamical system the mass distribution is described by the form of theoretically existent orbits $(\vec{x}(t), \vec{v}(t))$. Position and

velocity are linked with six coordinates and contain all information about the potential. With Newton's 2nd law we get the connection between potential $\Phi(\vec{r})$and acceleration $\vec{a}$ which is

$$\vec{\mathrm{F}}(\vec{\mathrm{r}}) = -\nabla\Phi(\vec{\mathrm{r}}) = \mathrm{m} \cdot \vec{\mathrm{a}}.$$

gcs are collisional clusters but we assume them as collisionless
time evolution of actions

2.4.2 The effective potential

The pericenter $\mathrm{r_{min}}$ and the apocenter $\mathrm{r_{max}}$ as well as the guiding star radius $\mathrm{r_g}$ can be found in the effective potential

$$\Phi_{\mathrm{L}}(\mathrm{r}) = \Phi(\mathrm{r}) + \frac{\mathrm{L}^2}{2\mathrm{r}^2}. \tag{6}$$

which is dependent on the Centrifugal potential $\mathrm{L}^2/2\mathrm{r}^2$ whit the angular momentum L (taken from Bartelmann (2008, p. 59, eq. 6.27)). In the peri- and apocenter the effective potential equals the total energy since the stars do not have any kinetic energy there. That results in following function which is to solve:

$$\left(\frac{1}{\mathrm{r}}\right)^2 + \frac{2 \cdot (\Phi(\mathrm{r}) - \mathrm{E})}{\mathrm{L}^2} = 0.$$

The guiding star radius is the distance at which a star with given total angular momentum would have a circular orbit. This is at the minimum of the effective potential. To get r_g we have to solve

$$r\sqrt{r\frac{\partial\Phi}{\partial r}} - |L| = 0$$

where $\sqrt{r\frac{\partial\Phi}{\partial r}} = v_{circ}$ is the circular velocity. This distance is used to have a better comparison of the actions since in the snapshot the stars are at a random position on their orbit.

2.4.3 Actions

Stars in spherical symmetric potential are fully described by their actions

$$J_i = \frac{1}{2\pi}\oint_{\gamma_i} \vec{p} \cdot d\vec{q} \qquad\qquad i = r, \theta, \phi \tag{7}$$

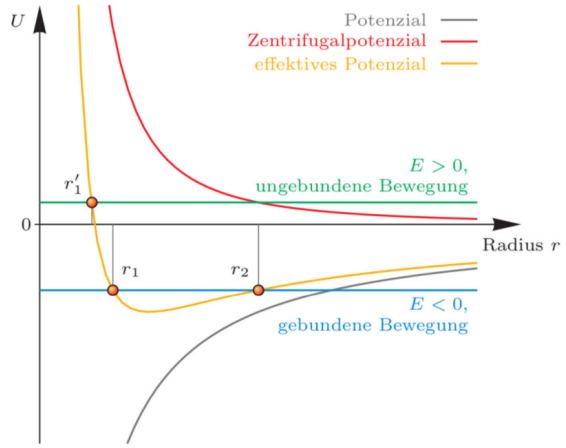

(a) General potential of a central field. The black line is the potential which is the difference between the effective potential (yellow line) and the centrifugal potential (red line). If the effective potential is positive the object is unbound while having a negative potential the object moves on a bound orbit. The points where the effective potential equals the total energy are the peri- and apocentre (r_1 and r_2) of the orbit. The point with the lowest effective potential is the guiding star radius. This is the distance a star with given angular momentum would have on a circular orbit. [Bartelmann Skript Theo 1]

Plots/pot_eff_theory_part.pdf

(b) Effective potential of a random star of SIM 1 (blue line). The total energy of the star (red line) is -1.88e-24 pc^2/s^2. The intersections of energy and effective potential are the peri- and the apocentre of the star (magenta and black lines) and the minimum of the effective potential (green line) is the guiding star radius.

Figure 3: Effective potentials.

which are used as coordinates in action space These actions are integrals of motion. For most potentials actions can't be described analytically. The actions of a spherical system are derived from angular momentum, energy and potential. Only the potential is depending in r. Energy and angular momentum as well as resulting actions are constant over time and orbit. The azimuthal action J_ϕ and the latitudinal action J_θ can be evaluated simply. To calculate the radial action J_r we have to solve an integral numerically. Actions of a spherical potential are found to be

$$J_\phi = L_z, \tag{8}$$

$$J_\theta = L - |L_z|, \tag{9}$$

$$J_r = \frac{1}{\pi} \int_{r_{min}}^{r_{max}} \mathrm{d}r \sqrt{2E - 2\Phi(r) - \frac{L^2}{r^2}}. \tag{10}$$

Should I write down the derivation of the actions (B&T p.220) or just the results (B&T p.221, 3.221,3.223,3.224)?

2.4.4 Numerical orbit integration

To deriver the potential solve the integrals of the Poisson's equation (5) numerically by using the Gauss-Legendre quadrature

$$\int_a^b f(x)dx = \frac{b-a}{2} \sum_{i=1}^{n} w_i f\left(\frac{b-a}{2} x_i + \frac{a+b}{2}\right)$$

where the points x_i and the weights w_i are derived from the Legendre polynomials and a and b are the integration limits.
Since the orbit is described by position and velocity at each time step we use the numerical leapfrog method which is a second-order time reversible integrator. X_i and v_i are calculated by

$$x_{i+1} = x_i + v_i \Delta t + \frac{a_i(x_i)}{2} \Delta t^2$$

$$v_{i+1} = v_i + \frac{a(x_{i+1}) + a(x_i)}{2} \Delta t.$$

2.5 Examples for orbits in spherical potentials

3 Analysis

3.1 Description of the simulation

We consider a set of Monte Carlo cluster simulations, developed with the Monte Carlo code MOCCA of Hypki and Giersz (2013)Hypki et al. 2013 (see also Giersz (1998) is that the right one? Giersz et al. 1998). The simulations include an initial mass function, stellar evolution, primordial binaries, and a relatively high number of particles, providing a realistic description of the long-term evolution of GCs with a single stellar population.

All the simulation had a metallicity of [Fe/H]=−1.3 and a Kroupa (2001) which one? initial mass function. The first simulation (from Giersz *et al.* (2015) right one? Giersz et al. 2015, kindly shared by the authors) contain an IMBH of $10^4\,M_\odot$ and its initial condition is drawn from a King model with concentration parameter W_0=6, $6.9\cdot10^5$ initial number of particles, 95 % of which are binary systems. We consider two snapshots of the simulation on at 10 and one at 7 Gyr. We call these snapshots SIM1-IMBH and SIM2-IMBH, respectively. Other two simulations (from Downing et al. 2010Downing *et al.* (2010)this one? , kindly shared by the authors), do not contain an IMBH and have an initial number of particles of $5\cdot10^5$ and $2\cdot10^6$, 10 % of initial binaries, and initial conditions drawn from a Plummer (1911) model with a ratio between the initial tidal radius and half-mass radius of 75. We consider a 11 Gyr snapshot for both simulations and we call them SIM3-NOIMBH and SIM4-NOIMBH, respectively.

We summarize in Table 1 the properties of the simulations for the time-snapshots considered.

Name of the simulation	Number of particles	Total mass [$M_\odot$]	Mass of the IMBH [$M_\odot$]	r_m [pc]	Age [Gyr]
SIM 1 - IMBH	1026735	$3.09\cdot10^5$	10102	4.13	10
SIM 2 - IMBH	1079376	$3.26\cdot10^5$	8902.3	3.58	7
SIM 3 - NOIMBH	468627	$1.73\cdot10^5$	0	7.89	11
SIM 4 - NOIMBH	1851556	$6.70\cdot10^5$	0	5.41	11

Table 1: Overview of the data of the simulations. We show the basic properties of each simulation which are numper of particles, the total mass, the mass of the IMBH, the half mass radius and the age. The half mass radius is defined by the radius which includes half of the mass of the whole system.

The output of the simulations relevant for our work are for each star: the position vector x, the velocity vector v in Cartesian and polar coordinates, mass, luminosity, magnitude b and v band and whether the star is a binary or not.

We compute the half-mass radius r_m given in table 1 by calculating the distance where half of the mass of the GC is inside the sphere of given distance and half of the mass is distributed outside of this sphere. We need it to compare the different simulations since their actual distance is depending on the simulation and is therefore not comparable. To get familiar with the simulation we first have a look at the spatial distribution of the stars.

3.2 Investigation in color magnitude space

As mentioned in 2.1 the CMD is showing a star's evolution stage dependend on its position. If one do not know age or metallicity of the system isochrones can be fitted on the CMD. We plot several isochrones (see section 2.1) to our CMD to determine which one fits best. This will give us the age and the metallicity of the system.

3.3 Investigation in phase space

First we will investigate the GC in phase space for the set of simulations that we will use throughout this work. We will start with the velocity dispersion and the anisotropy parameter then we will have a density profile and from that get the potential.

3.3.1 Kinematics

With equation (1) from section 2.2 we can calculate the velocity dispersion in each coordinate direction $\sigma_r, \sigma_\theta, \sigma_\phi$. For every bin we take the same amount of stars and calculate the dispersion along the radius of the GC. As radial values we use the average radius of the stars falling in the bins. To compare all simulations we plot the dispersion over the distance in units of the half-mass radius. The half mass radii of the simulations can be taken from table 1. As expected there is a rise in the centre for the simulations with IMBH. This is due the high gravitational potential of the IMBHs which disturbs the dynamics of close stars. The rise is equally visible in all three velocity components. This is since the kinematics are isotropic in the centre of the GC (see figure 8). There is no difference in the polar and the azimuthal velocity dispersion profiles because the system is spherical. In the outer regions the radial velocity dispersion decreases linear while the tangential slope becomes less steep. The motion in the outer angular shells seems to be different to the motion in radial direction.

In 7 we noted a difference in the radial and in the tangential velocity dispersion. To properly quantify that difference we consider the anisotropy profile. Anisotropy can

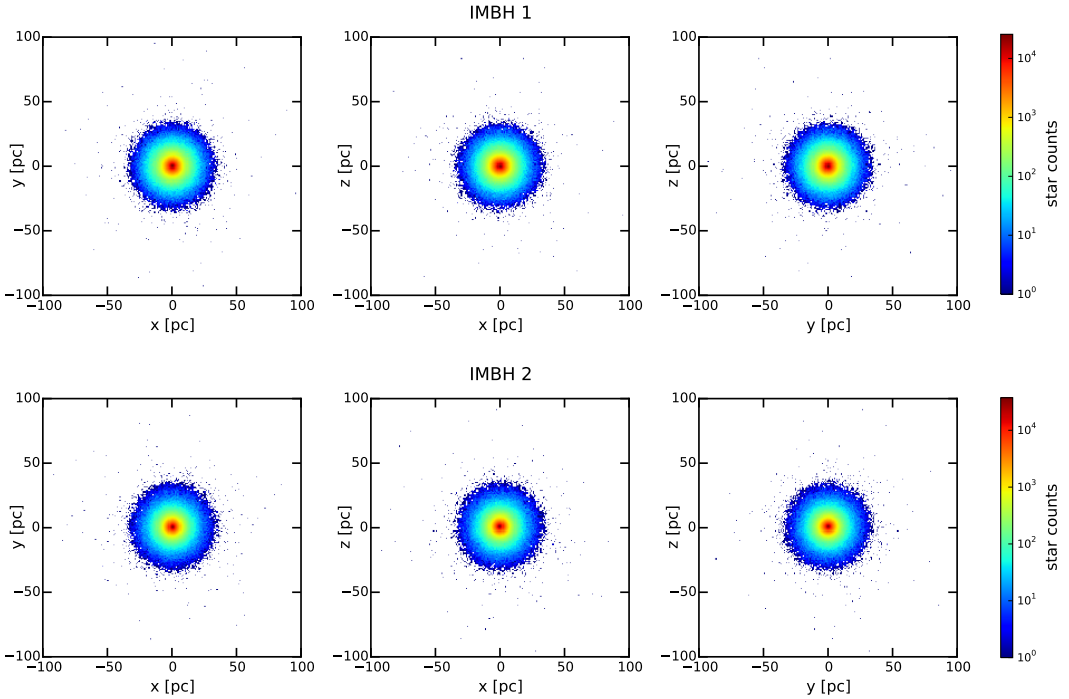

(a) SIM 1 & SIM 2. The GCs are spread until 100 pc with most of the stars located in the inner 40 pc.

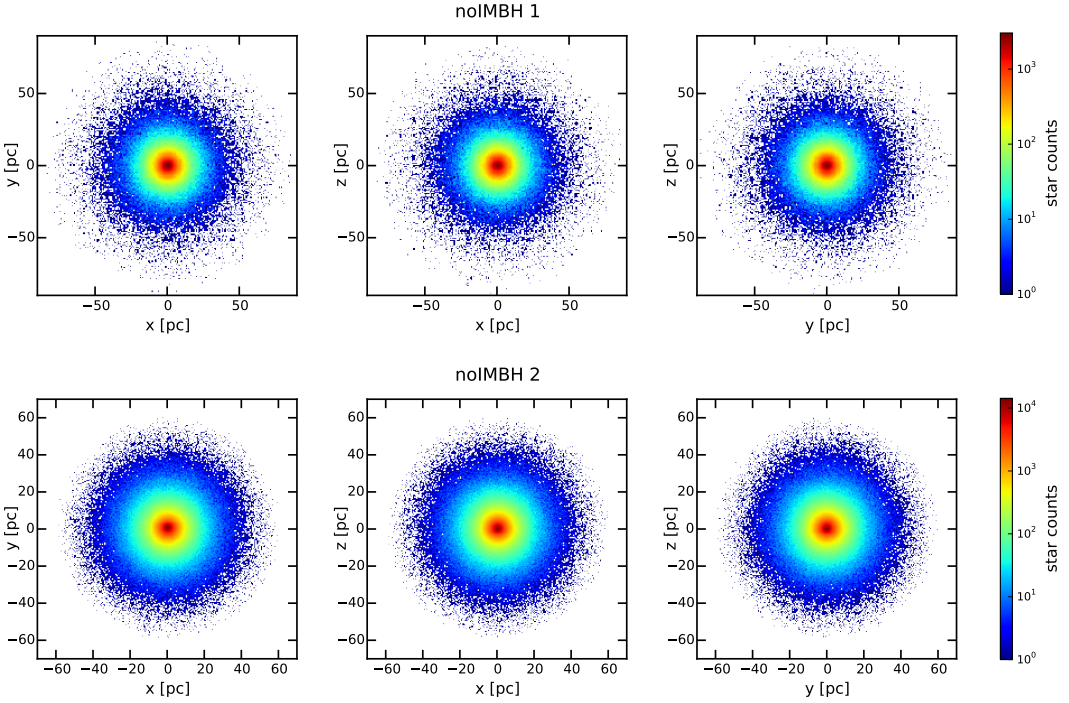

(b) SIM 3 & SIM 4. The GC is spread until 90 pc (SIM3) and until 60 pc (SIM4).

Figure 4: Spatial distribution of stars in the simulated GCs. The stars are distributed spherically with most of the stars in the inner part. The stars of the GCs with IMBH are less spread in the outer parts except very few which are far outside. This is simply due to the different initial concentration conditions of the simulations. In the GCs without IMBH the stars in the outer part are less accumulated but the furthermost stars still in the main sphere.

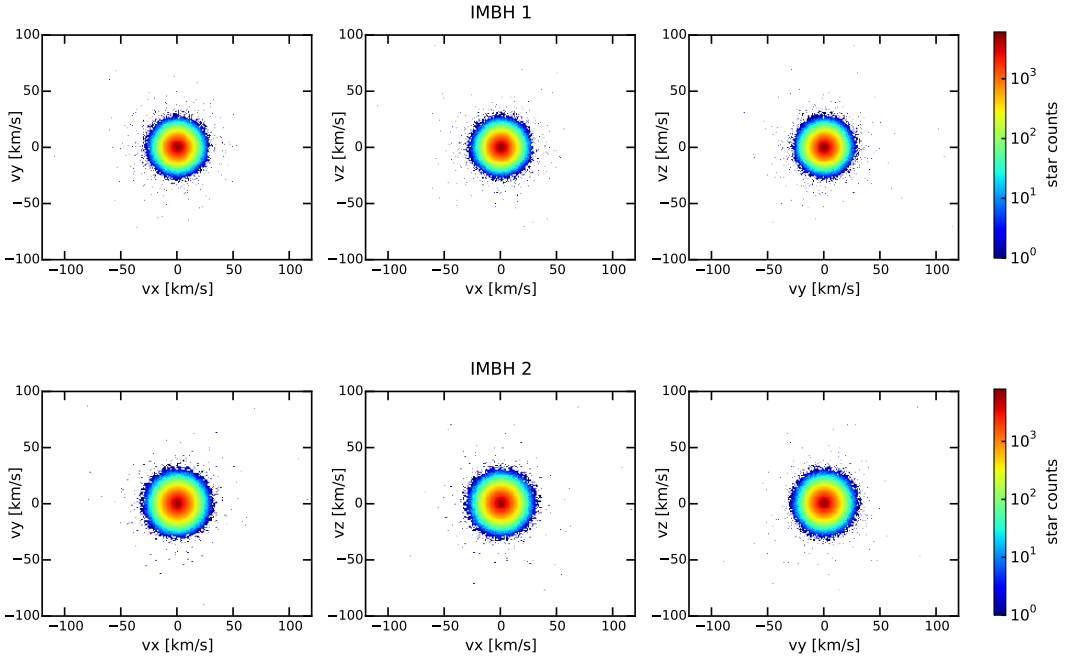

(a) SIM 1 & SIM 2. The stars' velocities are spread until 120 $^{\mathrm{km}}/_{\mathrm{s}}$ with most of them reaching 30 $^{\mathrm{km}}/_{\mathrm{s}}$.

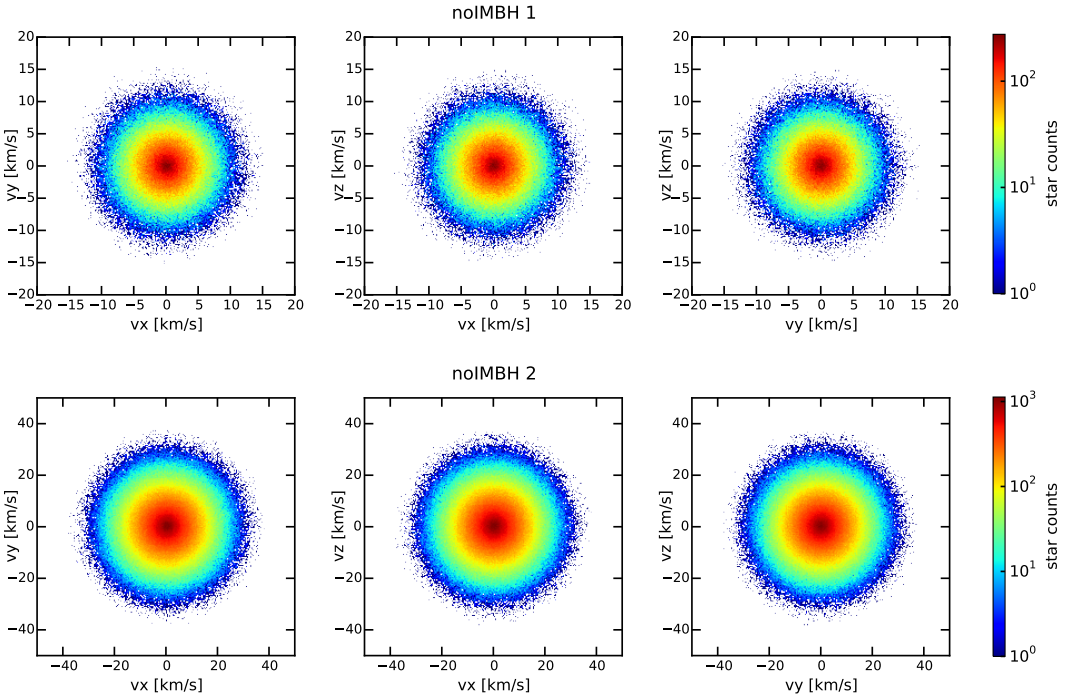

(b) SIM 3 & SIM 4. The stars' velocities are spread until 15 $^{\mathrm{km}}/_{\mathrm{s}}$ for SIM 3 whereas they spread until 40 $^{\mathrm{km}}/_{\mathrm{s}}$ for SIM 4.

Figure 5: Velocity distribution of stars in the simulated GCs. The velocities are isotropically spread around $\vec{v} = 0$. Most of the stars have low or no velocity while a few have high velocities in different directions. There are no overall streaming motions.

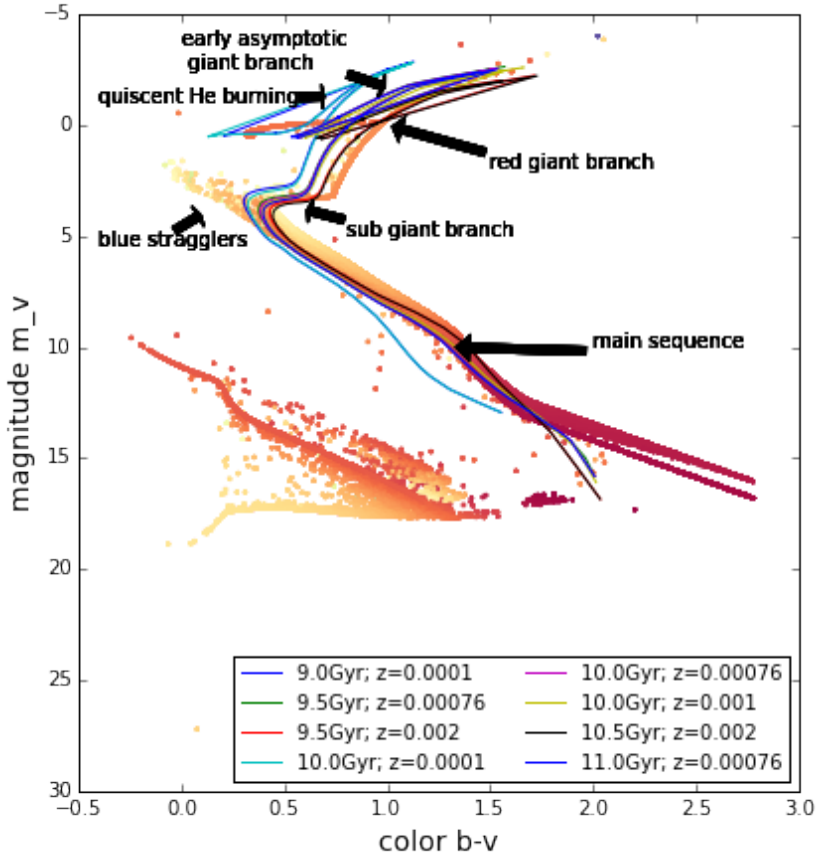

Figure 6: Color magnitude diagram of SIM 1 overplotted with different isochrones. We recognize how we can determine the age based on the turn off point. This verifies the age and the metallicity of this GC of 10 Gyr and 0.001.

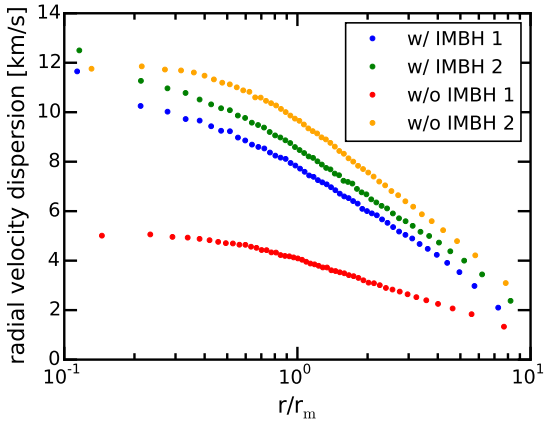

(a) Radial velocity dispersions

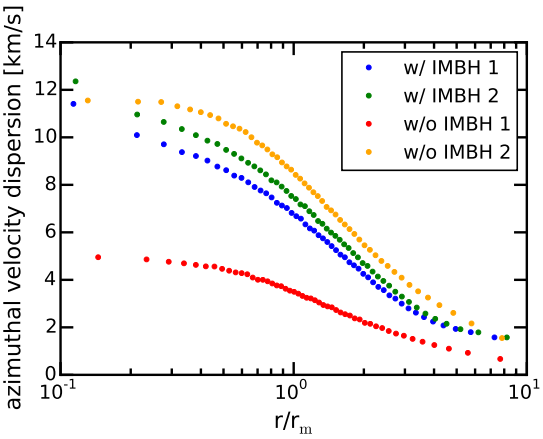

(b) Azimuthal velocity dispersions

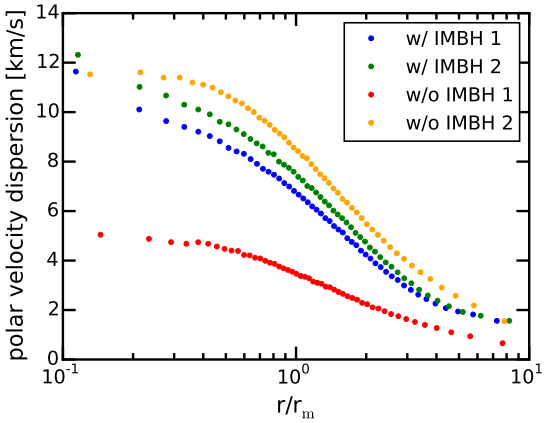

(c) Polar velocity dispersions

Figure 7: Velocity dispersion profiles of v_r, v_ϕ, v_θ as a function of the radius in units of the half-mass radius r_m. Blue and green points are the velocity dispersions of SIM 1 and 2 and the red and yellow ones are the velocity dispersions of SIM 3 and 4. They are binned in a way that each bin contains the same amount of stars. The given radius is the mean radius of the stars of each bin. We can see that the velocity dispersion of the simulations with IMBH rises towards the centre whereas the simulations without IMBH exhibits a cored profile.

be calculated from equation (2) in 2.2. Radial anisotropy means that there is higher velocity dispersion in radial direction than in angular direction. This comes probably along with a substantial number on eccentric orbits. The profile is binned the same way as the velocity dispersions and given in units of the half-mass radius. In the central

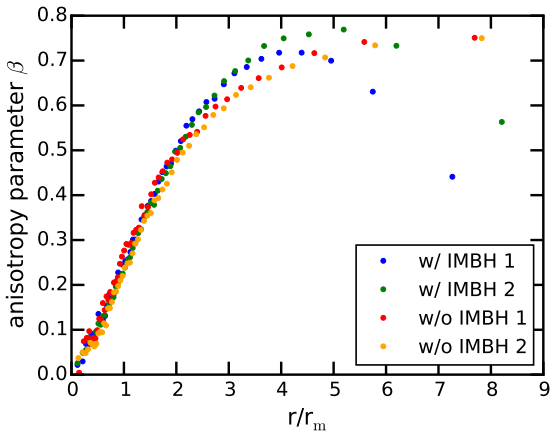

Figure 8: Profile of the anisotropy parameter β. The colors are given as in 7. All simulations are isotropic in the centre and become increasingly radial anisotropic in the intermediate regions. The simulations with IMBHs have a peak at 4 and 5 effective radii where they are most radial anisotropic. Some difference in anisotropy is observable between the simulations with and without IMBH. This is due to different truncation prescriptions used in the simulations. We note that within $\approx 2r_m$ all simulations exhibit the same anisotropy profile.

$\approx 2r_m$ of all GCs there is nearly the same anisotropy: isotropy in the centre & radial anisotropy while going in the outer parts. That means the systems are radial anisotropic. In the centre the anisotropy is zero. There the system is isotropic and the stars move in no preferred direction. The GCs with IMBH are most radially anisotropic at about 4 effective radii. The other GCs are becoming more radial anisotropic the further away from the centre it is. The difference is due to different truncation prescriptions of the simulation.

3.3.2 Spatial distribution

It is important to determine the density distribution for several reasons:

milar to each other

l (see section 2.3.3)

•

The density profile shows the density calculated by equation (3) of the system over its radius. As bins we use radial shells with logarithmic spacing chosen so that they are at least 100 stars per bin to have a reliable statistic. Outside of the cluster the density is set to 0. In the centre of the GCs (the distance of the 300th star of each simulation) we extrapolate the density profiles by setting it to the constant value of the innermost shell.

We try to find a analytic fitting function to the density profile for SIM 1 to calculate the potential from the Poisson's equation (4). We use two variations of an exponential function which could fit well. Also we want to check if the density follows a classical GC profile which i.e. is the Plummer profile. In Figure 9b we see that we can not find a simple fitting function nor a classical profile which describes the density. To get a analytical function we continue by using the interpolated density given in Figure 9c.

We test the sphericity of the GC and its centre of mass (COM). Sphericity allows the usage of analytical methods that are very straight forward, especially for determing the potential of the globular cluster and from that the actions in action space. We will do this by splitting the GC into octants and compare their mass density profiles. As one can see they're acceptable overlaying within their errors . This is done first for the centre of the coordinate system. We do the same for the centre of mass which is calculated by formula insert formula in theory part somewhere and compare it in figure 10.

From the density profile we can compute the potential as described in 2.3. It is composed by the potential given from the stars and if there is one the potential of the IMBH expressed as Kepler potential.

3.4 Investigations in action space

After investigating the orbits at given actions and the time evolution of the integrals of motion we consider all actions and other integrals of motion at our given snapshots. We have a look at the energies and angular momenta of the stars and compare them with the radial actions. Our main goal is to find any systematic signatures for the simulations with IMBHs that can be considered as the direct evidence of the dynamical effect of the IMBH itself. For this reason we investigate selected stars which show an abnormal behaviour in above-mentioned plots and compare them to the rest of the data to see where we find them.

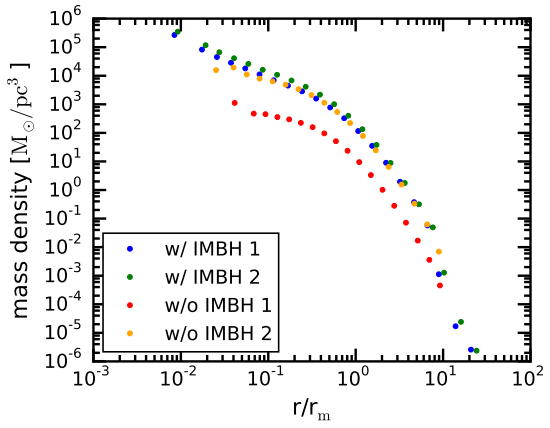

(a) Mass density profiles of all four simulations.

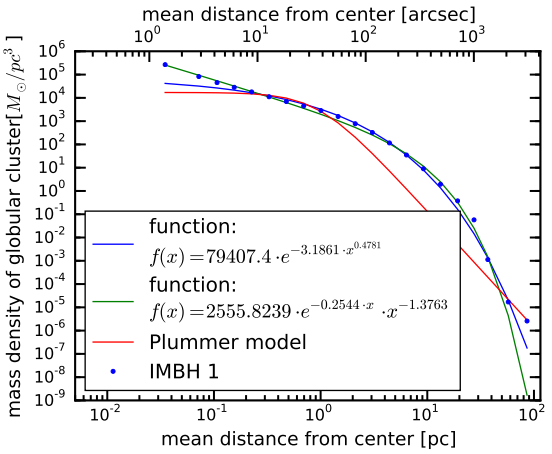

(b) Analytically fitted mass density profile of SIM 1.

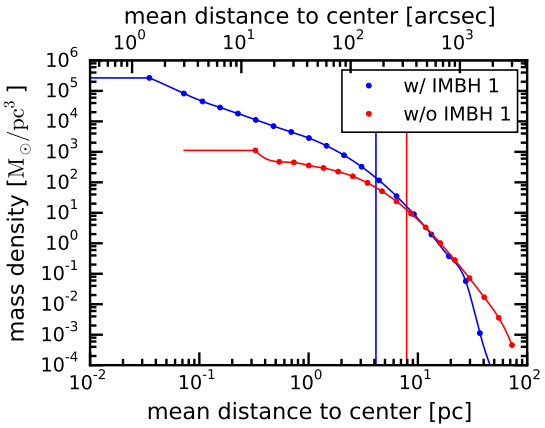

(c) Interpolated mass density profiles of SIM 1 and SIM 3.

Figure 9: Mass density profiles. The density in $\frac{M_\odot}{pc^2}$ is plotted against the effective radius. The density of the GC with IMBH is everywhere larger than the density of the GC without IMBH. In the centre there is a raise in the density of the GC with IMBH whereas the other GC stays approximately on the same level. Both start decreasing at about 0.5 r$_e$ff. We can see in Panel 9c that it is not simple to find an analytical function describing the density globally for both low & high radius. That is why we interpolate it in Panel 9c. Everything out of the GC is set to 0 while the innermost density is set to be the value of the innermost point.

Figure 10: Test for sphericity and center of mass of SIM 1.

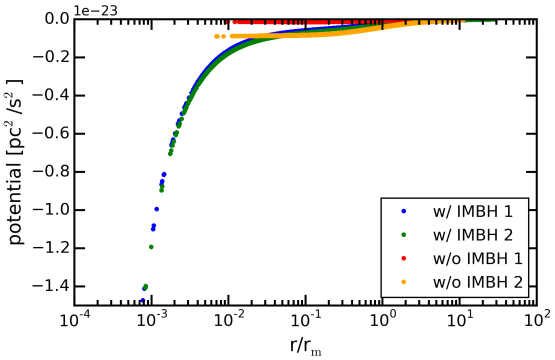

Figure 11: Potential of all GCs. SIM 1 and SIM 2 are nearly overlaying. They are the same simulation at different ages. The simulation lost 5 % of its stars with 10 % of the total mass while the IMBH gained 13 %. The potential of the stars declines while the potential of the IMBH rises so the potential stays the same. The GCs without IMBH remain constant in the inner part (until 0.5 half mass radii) and decrease from the points where their densities decrease.

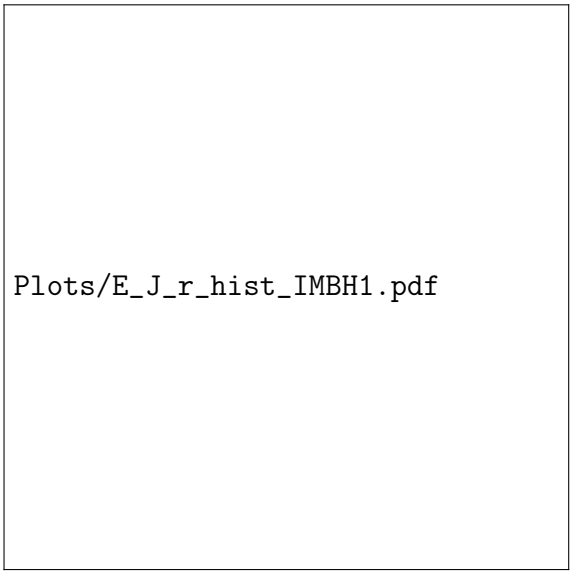

(a) SIM 1

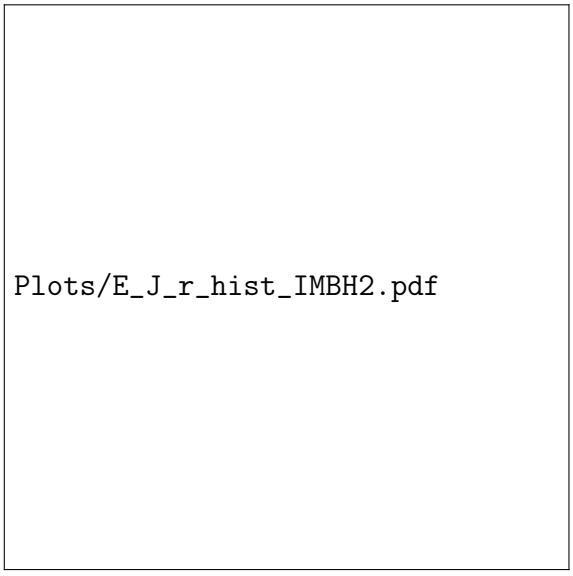

(b) SIM 2

(c) SIM 3

(d) SIM 4

Figure 12: Radial action over energy. In 12a and 12b it is plotted for both simulations with IMBH and the lower ones are for the simulation without IMBH. We find the crescent shape from 12c and 12d clearly in 12a and 12b. But in SIM 1 and SIM 2 there are some stars differing from this shape. Some have high energy with no radial actions (henceforth referred to as group 1) while others have high radial actions with nearly no energy (henceforth group 2).

(a) Star of group 1

(b) Star of group 2

Figure 13: Effective potential of exemplary stars of both groups from figure 12. The star of group 1 is clearly one a circular orbit with $r_{min} \approx r_g \approx r \approx r_{max}$. The star of group two has a highly eccentric orbit and its actual position is in its apocentre.

3.4.1 Energy

In 12 we plot the radial action over the energy of the star as histograms for all GCs. We see clearly some stars outside of the moon shape. They have either no radial action and high energy(below $-4 \cdot 10^{-24}\ pc^2/s^2$) or nearly no energy and high radial action (above 500 pc km/s).

We check the effective potential of the stars of the group to get information of their orbits and their actual positions. In 13 show one exemplary graph for each group taken from SIM 1.

The first group of stars of SIM 1 contains 38 of the nearest 110 stars including the innermost 15 stars. Since they have really low (nearly 0) radial actions they are on circular orbits. The nearest 15 on circular orbits around the IMBH are certainly locked to the IMBH. That is why we do not see this signature for SIM 3 and SIM 4. The other stars of this group are likely to be locked to the IMBH as well while the rest of the near stars which are not in this group seem to be near to or in their pericentre on more elliptic orbits and therefore not locked to the IMBH.

The other group of stars with high radial actions and nearly no energy can not be clearly related to the IMBH. They are the furthermost stars of the snapshot. All are

in their apocentre on very elliptic orbits (calculate ellipticity?). This ellipticity could be caused by the IMBH but since most of their pericentres are at a few pc we can not assume much interaction with the IMBH for those stars. Another reason that these stars do not occur in this way in SIM 3 and SIM 4 can be due to different truncation prescriptions used in the simulations (see graph 8). These stars are nearly outside of the GCs and have about zero energy so they could have been excluded in SIM 3 and SIM 4.

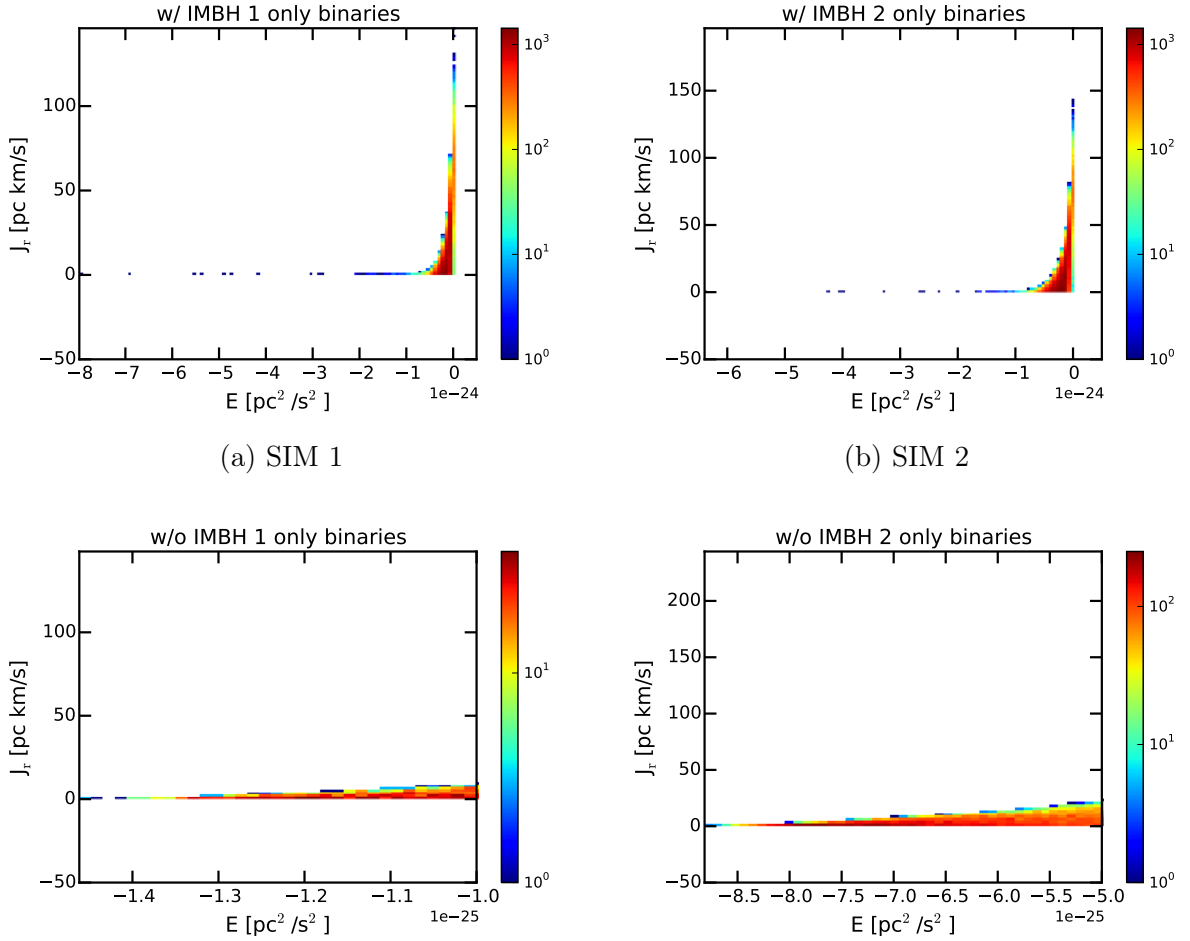

(a) SIM 1

(b) SIM 2

(c) SIM 3

(d) SIM 4

Figure 14: Radial action over energy only of binary systems. We see the same distribution of stars as in 12.

We might get these high energies from former binaries which were divided earlier. One of the stars could have been captured on a circular orbit near the centre while the other could have been left on an unbound orbit and have left the system. To check this we will plot the same values only for our actual binary systems. As we see in 14 the binary systems are behaving like single stars. There is no signature that the divergent stars are

leftovers of former binaries.

3.4.2 Angular momentum

Next we plot the radial actions over the absolute angular momenta of the stars of the simulations again as histograms. In 15 we can see a triangular shape which seems characteristic. Inside this shape we see some substructure in the GCs with IMBH. The stars outside the shape are the stars of group 2 which we see in 12 and 14 as the stars with no energy and high radial actions. Obviously they don't seem to have a specific angular momentum. We do not know how to identify the stars in the substructure. There could be a mass-dependent correlation due to dynamical mass segregation.

3.4.3 Guiding star radius

We extract these divergent stars and determine their properties. First we check the positions of their actions depending on their guiding star radii. In graph 17 the radial actions are plotted over their guiding star distances. We highlight the stars of group 1 and group 2 taken from graph 12 for SIM 1 and SIM 2. In general, there are several stars which have a really small guiding star radius (up to $10^{-}5\,\mathrm{pc}$). In SIM 3 and SIM 4 only very few stars go below 0.1 pc. Another difference between the GCs with and the ones without IMBH is that on the right border the lower end goes until very low radial actions for SIM 1 and SIM 2 (up to $10^{-}6\,{}^{\mathrm{pc\ km}}/_{\mathrm{s}}$) while SIM 3 and SIM 4 end there softly at about $10^{-}2\,{}^{\mathrm{pc\ km}}/_{\mathrm{s}}$.

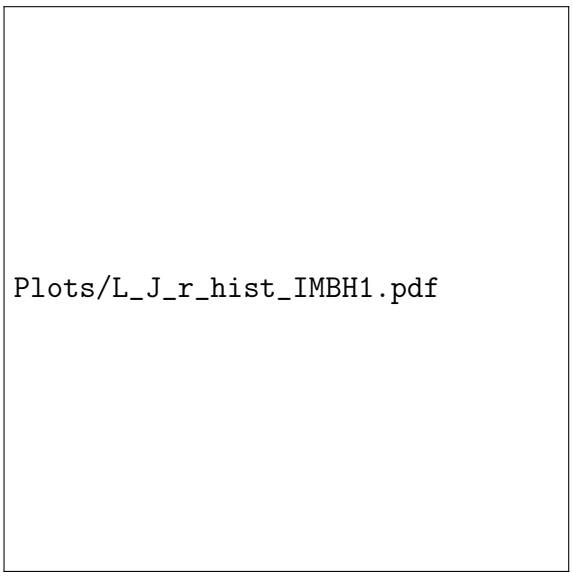

(a) SIM 1

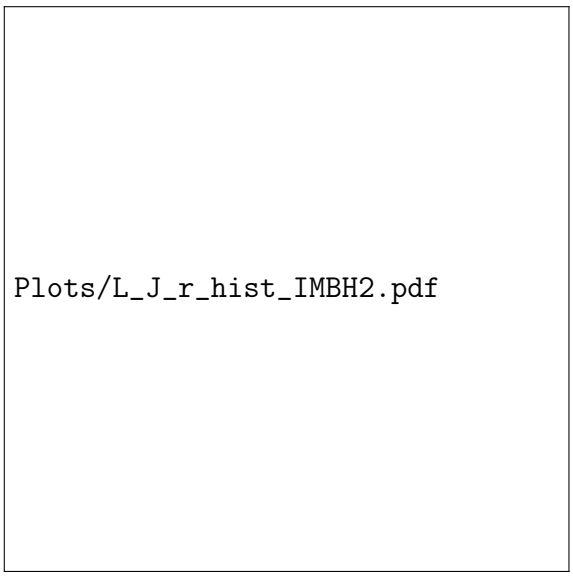

(b) SIM 2

(c) SIM 1 mass weighted

(d) SIM 2 mass weighted

(e) SIM 3

(f) SIM 4

Figure 15: Radial action over angular momentum. 15e and 15f look again very similar to each other with no recognizable substructure. In 15a and 15b there are stars above the main shape. In the shape we can clearly see a substructure

(a) Radial action over energy only for IMBH influenced stars of SIM 1.

(b) Radial action over energy only for IMBH influenced stars of SIM 2.

(c) Radial action over angular momentum only for IMBH influenced stars of SIM 1.

(d) Radial action over angular momentum only for IMBH influenced stars of SIM 2.

Figure 16: Check for group 1 stars.

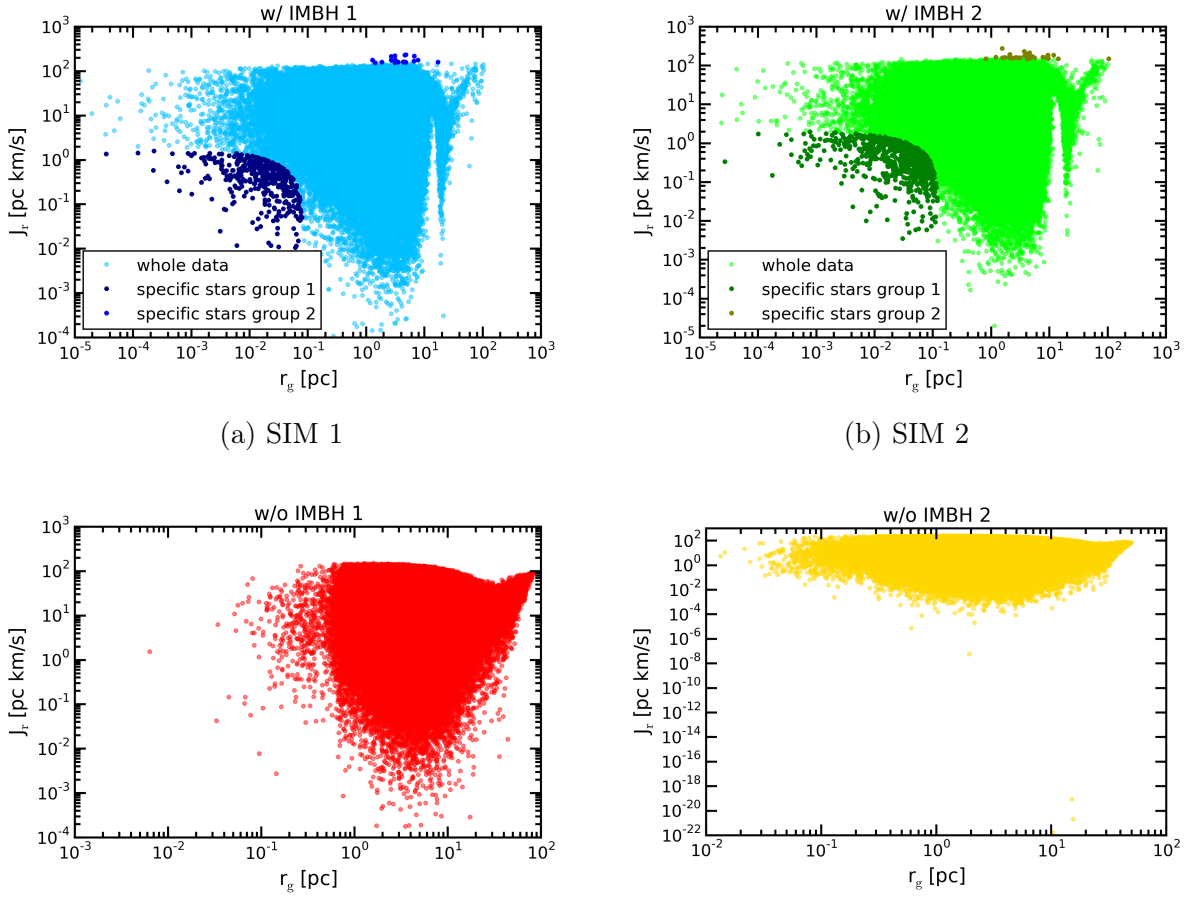

(a) SIM 1

(b) SIM 2

(c) SIM 3

(d) SIM 4

Figure 17: Radial action over guiding star radius with marked specific stars on loglog scale. All simulations have a similar shaped distributions except for the marked stars which are the specific ones. On the top right corner the shape of 12a and 12b is not gently rounded but there are single stars around it. On the lower left there are some extra stars which we identify as the stars with low radial action.

4 Results & Discussion

4.1 Signatures of IMBHs in action space

4.2 Discussion & future perspectives

In summary we can say that we found clearly evidence of the IMBH in the radial actions. To get there we made some simplified assumptions which should be investigated more precisely in an extended work. The density is the basis of our approach of the actions. Since we didn't find an analytical function we interpolated the binned densities and set the central density equal to the innermost density bin. Another attempt to get the density could be done by modelling Multi-Gaussian Expansion to the graph. But for this thesis we see the interpolation as sufficient since tests with some different densities do not destroy the figures of section 4.1.

Additional inaccuracy of the results rises due to different simulations for GCs with and without IMBH. Since they have different initial conditions and conditions throughout the simulating process we can not compare them directly. Especially the radial actions can not be compared since they are mass dependent. We see the differences directly in the scatter plots (figures 4 and 5) and in the anisotropy due to different truncation prescriptions. In further investigations we should consider using simulations with same conditions despite only the absence of an IMBH in one of the simulations.

Some physical assumptions have been that actions stay totally constant over time or rather that we have only looked at them at the time of the snapshot (despite a few stars for which we integrated the orbit and have looked at the time evolution of their integrals of orbits). Changing integrals of motion go along with changing orbits which could have some numerical fluctuations especially near the IMBH.

Another assumption is that we use specific values if not said else. That means we divide all values by the mass of the stars. We see in fig 15 that there can be distortion due to that. Further work can investigate the mass dependency of the integrals of motion.

If all these points are applied to this method we should think of a way to apply this approach to observational-like data. The main difference is that at this moment there is no possibility to get the masses of the stars of GCs and therefore we can not derive the potential which is essential for this method.

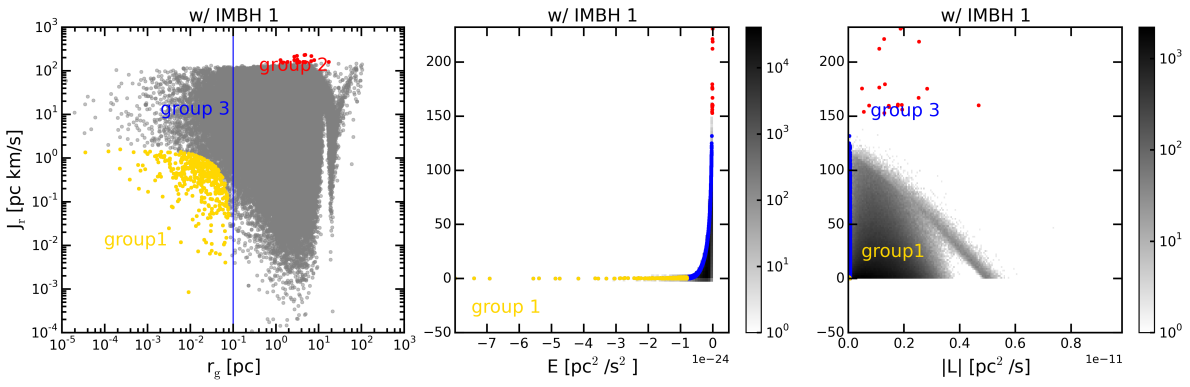

Figure 18: Radial action over different values.

5 Acronyms

CMD color magnitude diagram

COM centre of mass

DF distribution function

GC globular cluster

HST Hubble Space Telescope

IMBH intermediate mass black hole

MW Milky Way

SMBH super massive black hole

SSP single stellar population

References

Bahcall, J.N. and Wolf, R.A. "Star distribution around a massive black hole in a globular cluster". ApJ, **209**, 214–232, 1976.

Bartelmann, M. "Theoretische Physik I: Punktmechanik und mathematische Methoden". 2008.

Bianchini, P., Norris, M.A., van de Ven, G., and Schinnerer, E. "Understanding the central kinematics of globular clusters with simulated integrated-light IFU observations". MNRAS, **453**, 365–376, 2015.

Bianchini, P., Varri, A.L., Bertin, G., and Zocchi, A. "Rotating Globular Clusters". ApJ, **772**, 67, 2013.

Binney, J. and Tremaine, S. *Galactic Dynamics: Second Edition.* Princeton University Press, 2008.

Carroll, B.W. and Ostlie, D.A. *An introduction to modern astrophysics and cosmology.* 2006.

Downing, J.M.B., Benacquista, M.J., Giersz, M., and Spurzem, R. "Compact binaries in star clusters - I. Black hole binaries inside globular clusters". MNRAS, **407**, 1946–1962, 2010.

Ferrarese, L. and Merritt, D. "A Fundamental Relation between Supermassive Black Holes and Their Host Galaxies". ApJ, **539**, L9–L12, 2000.

Giersz, M. "Monte Carlo simulations of star clusters - I. First Results". MNRAS, **298**, 1239–1248, 1998.

Giersz, M., Leigh, N., Hypki, A., Lützgendorf, N., and Askar, A. "MOCCA code for star cluster simulations - IV. A new scenario for intermediate mass black hole formation in globular clusters". MNRAS, **454**, 3150–3165, 2015.

Harris, W.E. "A Catalog of Parameters for Globular Clusters in the Milky Way". AJ, **112**, 1487, 1996.

Hypki, A. and Giersz, M. "MOCCA code for star cluster simulations - I. Blue stragglers, first results". MNRAS, **429**, 1221–1243, 2013.

Kacharov, N., Bianchini, P., Koch, A., Frank, M.J., Martin, N.F., van de Ven, G., Puzia, T.H., McDonald, I., Johnson, C.I., and Zijlstra, A.A. "A study of rotating globular clusters. The case of the old, metal-poor globular cluster NGC 4372". A&A, **567**, A69, 2014.

Kirsten, F. and Vlemmings, W.H.T. "No evidence for a central IMBH in M 15". A&A, **542**, A44, 2012.

Lanzoni, B., Mucciarelli, A., Origlia, L., Bellazzini, M., Ferraro, F.R., Valenti, E., Miocchi, P., Dalessandro, E., Pallanca, C., and Massari, D. "The Velocity Dispersion Profile of NGC 6388 from Resolved-star Spectroscopy: No Evidence of a Central Cusp and New Constraints on the Black Hole Mass". ApJ, **769**, 107, 2013.

Lützgendorf, N., Kissler-Patig, M., Gebhardt, K., Baumgardt, H., Noyola, E., de Zeeuw, P.T., Neumayer, N., Jalali, B., and Feldmeier, A. "Limits on intermediate-mass black holes in six Galactic globular clusters with integral-field spectroscopy". A&A, **552**, A49, 2013.

Lützgendorf, N., Kissler-Patig, M., Noyola, E., Jalali, B., de Zeeuw, P.T., Gebhardt, K., and Baumgardt, H. "Kinematic signature of an intermediate-mass black hole in the globular cluster NGC 6388". A&A, **533**, A36, 2011.

Maccarone, T.J. and Servillat, M. "Radio observations of NGC 2808 and other globular clusters: constraints on intermediate-mass black holes". MNRAS, **389**, 379–384, 2008.

Meylan, G. and Heggie, D.C. "Internal dynamics of globular clusters". A&A Rev., **8**, 1–143, 1997.

Miller, M.C. and Hamilton, D.P. "Production of intermediate-mass black holes in globular clusters". MNRAS, **330**, 232–240, 2002.

Mohr, P.J., Newell, D.B., and Taylor, B.N. "CODATA Recommended Values of the Fundamental Physical Constants: 2014". *ArXiv e-prints*, 2015.

Piotto, G., Milone, A.P., Bedin, L.R., Anderson, J., King, I.R., Marino, A.F., Nardiello, D., Aparicio, A., Barbuy, B., Bellini, A., Brown, T.M., Cassisi, S., Cool, A.M., Cunial, A., Dalessandro, E., D'Antona, F., Ferraro, F.R., Hidalgo, S., Lanzoni, B., Monelli, M., Ortolani, S., Renzini, A., Salaris, M., Sarajedini, A., van der Marel, R.P., Vesperini, E., and Zoccali, M. "The Hubble Space Telescope UV Legacy Survey of Galac-

tic Globular Clusters. I. Overview of the Project and Detection of Multiple Stellar Populations". AJ, **149**, 91, 2015.

Plummer, H.C. "On the problem of distribution in globular star clusters". MNRAS, **71**, 460–470, 1911.

Strader, J., Chomiuk, L., Maccarone, T.J., Miller-Jones, J.C.A., Seth, A.C., Heinke, C.O., and Sivakoff, G.R. "No Evidence for Intermediate-mass Black Holes in Globular Clusters: Strong Constraints from the JVLA". ApJ, **750**, L27, 2012.

Zocchi, A., Bertin, G., and Varri, A.L. "A dynamical study of Galactic globular clusters under different relaxation conditions". A&A, **539**, A65, 2012.